Structural, Thermodynamic, and Kinetic Properties of Alkali-Metal Intercalation into Group 5 Metal Ditellurides

R. Guzmán, J. Morales, and J. L. Tirado*

Laboratorio de Química Inorgánica, Facultad de Ciencias, Universidad de Córdoba, Avda. San Alberto Magno s/n, 14004 Córdoba, Spain

Received November 1, 1994. Revised Manuscript Received March 28, 1995[⊗]

Lithium and sodium intercalation into monoclinic tantalum ditelluride in A/$AClO_4$(PC)/$TaTe_2$ (A: Li, Na) electrochemical cells is reported. Lithium insertion takes place in successive steps by ordered filling of two types of distorted octahedral sites. Sodium insertion leads to new phases with $Na_{0.6}TaTe_2$ and $NaTaTe_2$ compositions and trigonal prismatic coordination of sodium ions due to the changes induced in the electron count of the d-block band. The structure changes, free energy of intercalation, average electrostatic repulsion factor of inserted ions, and chemical diffusion coefficients of the three isostructural group 5 ditellurides are compared. Lithium insertion is favored thermodynamically in these compounds while diffusion coefficients lower than those of sodium ions are found. $TaTe_2$ and $NbTe_2$ exhibit similar intercalation behavior which differs from that of VTe_2 in having more pronounced changes in unit-cell parameters, higher electrostatic repulsions between inserted sodium ions and lower intercalant diffusion coefficients.

Introduction

The structure and intercalation properties of layered transition-metal dichalcogenides have been the subject of extensive research for many years. However, a detailed understanding of the crystallographic and electronic structure of some of these systems has not been achieved until recently. An outstanding example is provided by group 5 transition-metal ditellurides (MTe_2, M: V, Nb, Ta). Although the crystallographic structure of $NbTe_2$ and $TaTe_2$ was described early on Brown,[1] the isostructural compound VTe_2 was studied in detail only some 18 years later.[2] Moreover, the d-electron count dependence of the structural modulations in these compounds was recently examined by using the concept of hidden 1-D bands.[3,4] According to this model, three 1-D bands result from the σ overlap of the in-plane metal t_{2g} orbitals along a, b, or $(a + b)$ directions in which edge-sharing octahedral chains run in an undistorted 1T structure. The distorted 1T-MTe_2 structure involves interlayer Te−Te interactions which increase the Te p-block band energy, thus favoring a d-electron count of metal ions close to $d^{4/3}$. The resulting band electronic structure can be described as two one-third filled hidden 1-D bands. This in turn, leads to trimerizations of the metal ions along, for example, the a and $(a + b)$ directions of the undistorted 1T structure (see Figure 1). The combined effects of these intralayer metal−metal interactions lead to metal ribbon chains running along the b direction. The in-plane supercell could be described by the parameters $a_p \simeq 3a_h$ and $b_p \simeq a_h$. In MTe_2 however, the ribbons of consecutive slabs

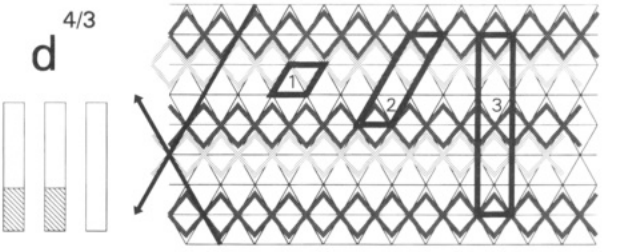

Figure 1. Filling of hidden 1-D d-block bands. The directions of the two half-filled bands are shown by arrows in a projection of vanadium ribbons corresponding to two consecutive MTe_2 layers. Tellurium atoms are omitted for clarity. The transition-metal atom positions in the undistorted 1T structure are shown by the intercept of thin lines. Labeled unit cells: (1) undistorted $a_h \times a_h$ basic structure; (2) in-plane $3a_h \times a_h$ superstructure; (3) complete monoclinic $3a_h3^{1/2} \times a_h$ structure.

are not superimposed, leading to the monoclinic $C2/m$ structure with $a_m \simeq 3a_h3^{1/2}$ and $b_m \simeq a_h$ (Figure 1).

On the other hand, an increasing number of layered transition metal dichalcogenides have proven adequate hosts for alkali-metal intercalation. The present knowledge of the structural, thermodynamic and kinetic properties of alkali-metal intercalation reactions extends from undistorted 1T and 2H dichalcogenides[5−8] to structurally more complex systems.[9] Concerning group 5 ditellurides, Murphy et al.[10] first described the chemical intercalation of lithium into $NbTe_2$ and $TaTe_2$

[⊗] Abstract published in *Advance ACS Abstracts,* May 1, 1995.

(1) Brown, B. E. *Acta Crystallogr.* **1966**, *20*, 264.
(2) Bronsema, K. D.; Bus, G. W.; Wiegers, G. A. *J. Solid State Chem.* **1984** *53*, 415.
(3) Canadell, E.; Jobic, S.; Brec, R.; Rouxel, J.; Whangbo, M. H. *J. Solid State Chem.* **1992**, *99*, 189.
(4) Whangbo, M. H.; Canadell, E. *J. Am Chem. Soc.* **1992**, *114*, 9587.
(5) Murphy, D. W.; Carides, J. N.; DiSalvo, F. J.; Cros, C.; Waszczak, J. V. *Mater. Res. Bull.* **1977**, *12*, 825.
(6) Basu, S.; Worrell, W. L. In *Electrode Materials and Processes for Energy Conversion and Storage*; Electrochemical Society: Princeton, NJ, 1977; p 861.
(7) Whittingham, M. S. *Prog. Solid State Chem.* **1978**, *12*, 41.
(8) Nagelberg, A. S.; Worrell, W. L. *J. Solid State Chem.* **1979**, *29*, 345.
(9) Hernán, L.; Morales, J.; Sánchez, L.; Tirado, J. L. *Chem. Mater.* **1993**, *5*, 1167.
(10) Murphy, D. W.; Di Salvo, F. J.; Hull, G. W.; Waszczak, J. *Inorg. Chem.* **1976**, *15*, 17.

0897-4756/95/2807-1171$09.00/0

Table 1. Unit-Cell Parameters of Pristine and Electrochemically Intercalated MTe_2 (M: V, Nb, Ta)

compound	a_m (Å)	b_m (Å)	c_m (Å)	β_m (deg)	V (Å^3)	c_h ($c_m \sin \beta_m$)	$a_m/3{\cdot}3^{1/2}{\cdot}b_m$
VTe_2	18.99_2	3.598_2	9.058_5	134.64_3	440	6.445	1.016
$NbTe_2$	19.24_1	3.630_2	9.269_4	134.47_2	462	6.615	1.020
$TaTe_2$	19.18_1	3.624_2	9.321_3	134.10_6	465	6.694	1.019
$LiVTe_2$	20.29_2	3.606_4	9.589_8	134.95_6	496	6.786	1.083
$LiNbTe_2$	19.45_1	3.751_5	10.00_1	133.91_5	526	7.204	0.998
$LiTaTe_2$	19.00_2	3.752_4	9.928_7	133.72_4	511	7.175	0.975
$NaVTe_2$	19.15_5	3.619_8	10.761_9	134.97_9	527	7.613	1.018
$NaNbTe_2$	3.64_1				92	8.01_1	1.000
$NaTaTe_2$	3.63_2				90	7.93_1	1.000

and a significant expansion of the pseudohexagonal c_h parameter was reported. More recently, the electrochemical lithium and sodium intercalation was studied in VTe_2[11] and $NbTe_2$.[12] Lithium intercalation into monoclinic VTe_2 takes place in several successive reduction steps corresponding to lithium intercalation processes by partial filling of the distorted octahedral sites in the interlayer space. For $LiVTe_2$, an expansion of the c_h parameter normal to the layers of ca. 0.35 Å was observed. Sodium intercalation led to lower cell voltages and greater interlayer expansions. Electrochemical lithium intercalation into 1T-$NbTe_2$ also takes place by progressive filling of the distorted octahedral sites. The monoclinic structure and niobium ribbon chain modulation are preserved during lithium intercalation. On the contrary, for $Na_{0.6}NbTe_2$, a $a_h27^{1/2} \times a_h27^{1/2}$ superlattice was observed.[12] The geometric relationships between ribbon chain and $3a_h \times 3a_h$ modulations in 1T-transition metal dichalcogenides are consistent with a trimerization of $3a_h3^{1/2} \times a_h$ modulations due to the changes in the d-band electron count and metal−metal bonding with intercalation. For $NaNbTe_2$, a fully intercalated phase with basal spacing of 8.01 Å and sodium ions in trigonal prismatic coordination has been observed.

This paper has a 2-fold aim: (i) the electrochemical lithium and sodium intercalation into $TaTe_2$ is reported, and (ii) the thermodynamic and kinetic properties of alkali-metal intercalation into the three compounds are compared.

Experimental Section

Powdered samples of the studied compounds were obtained by direct synthesis from the elements at 850 °C for 7 days (VTe_2) and 1000 °C for 4 days ($NbTe_2$ and $TaTe_2$) in evacuated silica ampules. Powdered metals and tellurium were supplied by Strem Chemicals.

The electrochemical intercalation of lithium and sodium was studied in A/1M $AClO_4$ in PC/telluride test cells (A: Li, Na). The electrochemical cells were prepared inside the drybox (M. Braun, water content ≤3 ppm) by placing a clean metal disk, two glass fiber separators soaked with the electrolyte solution and a pellet of the telluride concerned into a Teflon container with two stainless steel terminals. The cathode pellets (7 mm diameter, 0.3−0.5 mm thick) were prepared by pressing 12−20 mg of MTe_2 on an inert copper substrate (Merck, 99.7%). Galvanostatic intermittent titration technique (GITT) and step potential electrochemical spectroscopy (SPES) of the cells were carried out at 25 °C by using a multichannel microprocessor-controlled system (MacPile).[13] In all experiments, an initial relaxation of the cells was allowed until the condition $\Delta V/\Delta t \leq 1$ mV h^{-1} was attained. The SPES data were recorded with −10 mV h^{-1} voltage steps. Open-circuit voltage (OCV) composition curves were obtained by coulometric titration. Constant-current densities of 50 μA/cm^2 were applied to the cells for preset times so as to transfer known amounts of lithium and sodium into the crystals. After each titration, the cells were allowed to stand at open circuit to allow equilibrium to be restored, which was assumed to occur when the cell voltage changed by less than 1 mV in 1 h. All spectra were recorded in triplicate to ensure reproducibility. The average alkali-metal composition of the cathodic material was calculated from Faraday's law on the assumption that no current flow was due to side reactions.

X-ray powder diffractometry (XPD) was carried out using a Siemens D500 diffractometer furnished with Cu Kα radiation and a graphite monochromator. For intercalated phases, a plastic fiber was used to cover the sample in order to avoid undesirable reactions with air during the recording. Electron diffraction patterns were obtained on a JEOL 200 CX apparatus.

Results and Discussion

From XPD patterns of the as-prepared vanadium, niobium, and tantalum ditelluride samples, the monoclinic structure of the three compounds was evidenced by the splitting of the $P\bar{3}m1$ space group reflections of the basic CdI_2 structure, according to the reflection conditions of the $C2/m$ space group. In addition, the I_{001}/I_{002} intensity ratio increased from vanadium to tantalum, in agreement with the increasing scattering factor of the metal atoms inside Te−M−Te sandwiches. The observed unit cell parameters (Table 1) are in good correspondence with those reported by Brown[1] and Bronsema et al.[2] A larger departure from the hexagonal basic cell is found for $NbTe_2$ and $TaTe_2$ by comparing the $a_m/3b_m3^{1/2}$ ratio of the three compounds.

$\langle 001 \rangle_m$ Zone electron diffraction patterns of monoclinic 1T-$TaTe_2$ recorded with the electron beam lying almost perpendicular to the layers, i.e., almost parallel to $[001]_m$ rather than exactly parallel to it and close to the $[103]_m$ direction (Figure 2a), consist of alternate rows of $hk0$ spots that fulfill the $h + k = 2n$ condition of the $C2/m$ space group (Figure 2b). As in VTe_2[1] and $NbTe_2$[12], additional complexity of the pattern results from three sets of rows of satellite spots differing by 60°, suggesting that the particles consist of domains with three equivalent orientations. The pattern can also be regarded as the $[001]_h$ zone of the hexagonal basic structure including $P\bar{3}m1$ spots (connected by an hexagon in Figure 2b) and satellite spots of the in-plane $3a_h \times a_h$ superstructure. It should be emphasized that the monoclinic unit cell with $a_m \simeq 3b_m3^{1/2}$ results from the in-plane ribbon chain modulation and the fact that metal ribbons are not superimposed in consecutively stacked layers (Figure 1).

The GITT and SPES results for lithium and sodium cells using $TaTe_2$ as cathode material are compared in Figure 3. The complex discharge behavior of the cells

(11) Guzmán, R.; Morales, J.; Tirado, J. L. *J. Mater. Chem.* **1993**, *3*, 1271.
(12) Guzmán, R.; Morales, J.; Tirado, J. L. *Inorg. Chem.* **1994**, *33*, 3164.
(13) Chabre, Y. *J. Electrochem. Soc.* **1991**, *138*, 329.

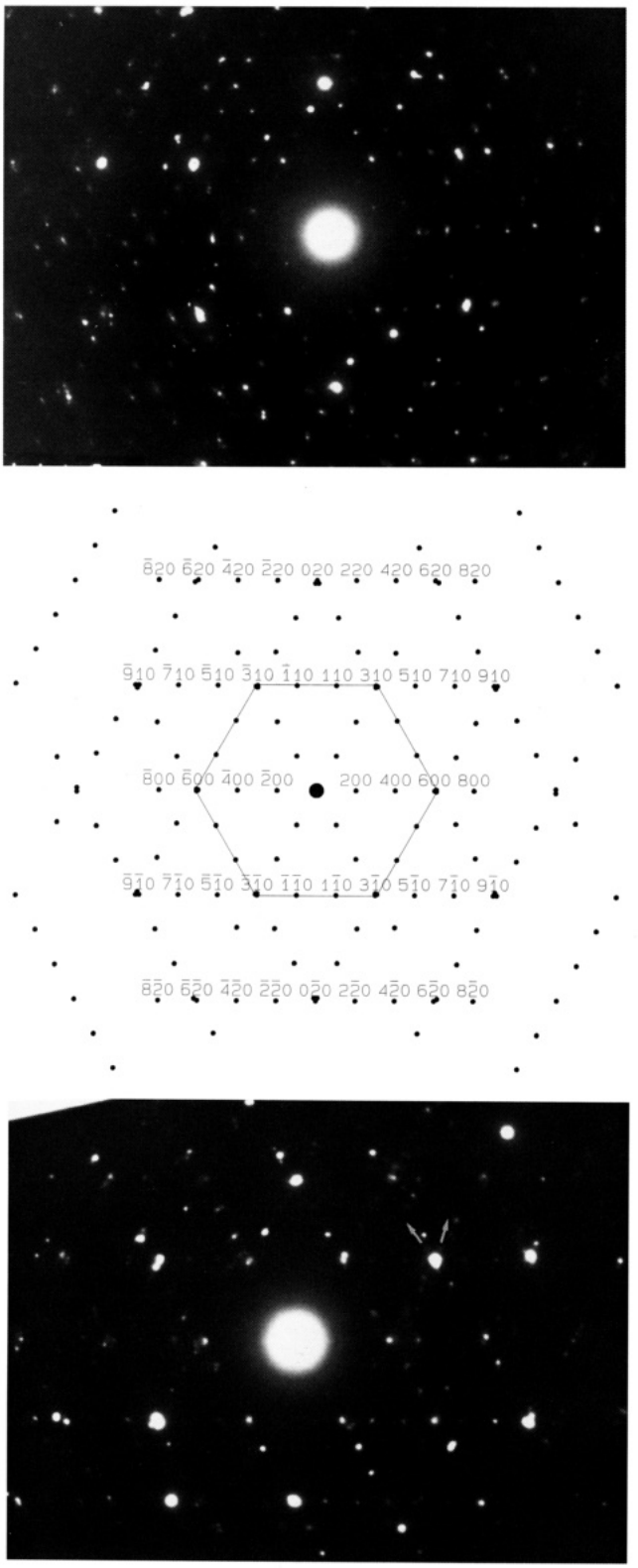

Figure 2. Electron diffraction patterns recorded with the electron beam lying almost parallel to the $\langle 001 \rangle_m$ zone axis in three equivalent orientational variants that are rotated by 60° with respect to each other, suggesting three equivalent domains. (a, top) $TaTe_2$; (b, middle) monoclinic labels of the spots corresponding to a single domain; (c, bottom) $Li_{0.2}TaTe_2$, small arrows show the direction in which extra satellite spots occur.

is evidenced by the presence of successive pseudoplateaus which may be associated with energetically different processes of lithium or sodium ion plus electron insertion. Consequently, well defined peaks occur in a plot of $-dx/dV$ vs x in galvanostatic mode and in the

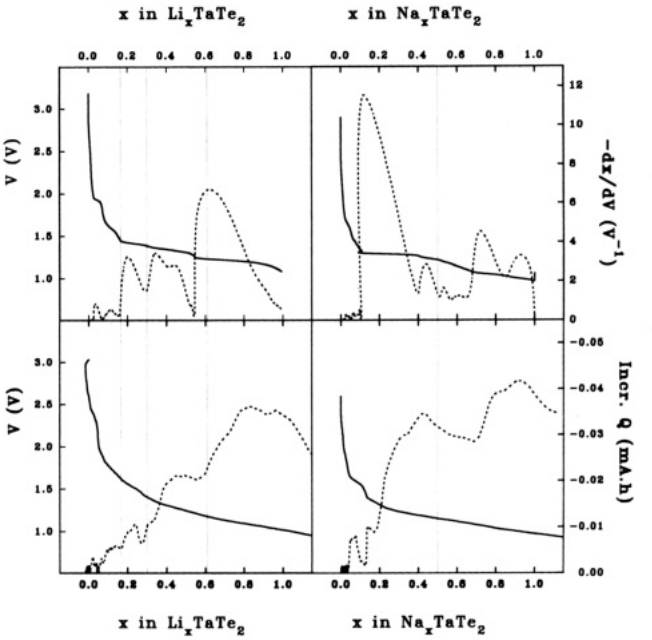

Figure 3. Results of galvanostatic intermittent titration (GITT, upper) and step potential electrochemical spectroscopy (SPES, lower) of $A/AClO_4(PC)/TaTe_2$ cells (A: Li, Na). Voltage vs composition curves in full line, $-dx/dV$ vs x and incremental capacity vs x curves in dashed lines. Vertical lines show composition limits for successive insertion processes.

corresponding incremental capacity vs x plots obtained by SPES. The location of the most relevant effects in these curves was assessed by the comparison of both techniques and the approximate limits of each process which is common to both types of plot are marked by vertical lines in Figure 3.

For electrochemical lithium insertion, a greater complexity is signalled by the occurrence of several consecutive pseudoplateaus located at 1.6, 1.4, 1.3, and 1.2 V with limits at x values of ca. 0.16, 0.33, 0.6, and 1.0, respectively. The last effect was followed by a marked decrease in voltage, which is consistent with a maximum degree of insertion close to $x = 1$, in good correspondence with the complete filling of the distorted octahedral sites located in the interlayer space of monoclinic $TaTe_2$. A slow relaxation of the current was observed in the vicinity of the incremental capacity peaks, which was indicative of slow diffusion after lithium ion plus electron injection processes.

The XPD patterns of cathode materials prepared by interrupting the discharge experiments showed the coexistence of pristine $TaTe_2$ and lithiated product, particularly for $x < 1$. Due to the diffusion of lithium ions in the complete mass of active material, sample homogeneity increased by allowing the products to stand inside the glovebox and single-phase products with intermediate parameters could be observed after several days. For $x = 1$, the XPD data (Table 2) were still indexable in the $C2/m$ space group, as a result of the topotactic nature of the process. The multidomain character of the particles is preserved during lithium intercalation as evidenced by the electron diffraction pattern obtained for $LiTaTe_2$, which is equivalent to that shown in Figure 2a.

For intermediate compositions, the peaks in the capacity curve may be correlated to the formation of ordered superstructures during the intercalation pro-

Table 2. Powder X-ray Diffraction Data of $LiTaTe_2$[a]

h	k	l	d_{obs}/Å	d_{calc}/Å	$(I/I_0)_{obs}$
0	0	1	7.20	7.17	100
6	0	−3	2.972	2.972	26
3	1	0	2.901	2.902	72
0	0	3	2.390	2.391	34
1	1	2	2.344	2.343	36
6	0	1	1.843	1.843	25
0	0	4	1.794	1.793	18
5	1	2	1.539	1.540	16
0	0	5	1.435	1.434	15

[a] Lines with $I/I_0 < 15\%$ are omitted.

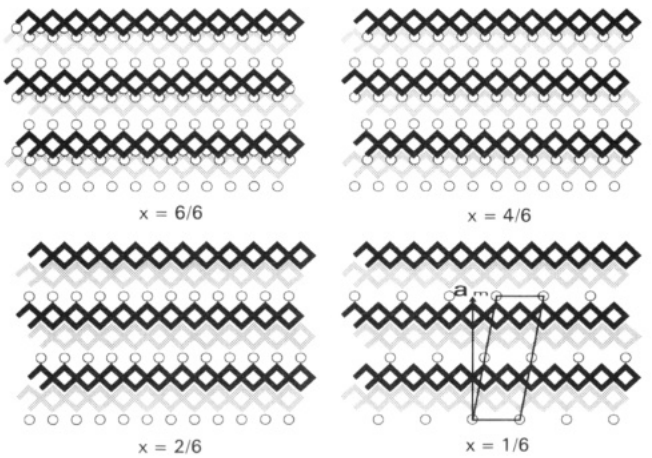

Figure 4. Schematic projection along [001] of ribbon chain clustering of metal atoms in two successive layers of $TaTe_2$ and partial occupancy of interlayer sites by lithium ions (○). For $x = 1/6$, the resulting unit cell runs parallel to the monoclinic [110] direction, forming 10.7° with the a_m vector.

cess.[14] Similarly, the peaks in the derivative of composition with respect to V may be interpreted by assuming ordered superlattices for the Li ions.[15] The good correspondence between the composition limits of these intermediates found by both electrochemical methods gives additional support to this interpretation. However, the possible occurrence of intermediate phases that could explain the complexity of the cell discharge was not shown by the XPD data of samples obtained at different depths of discharge. It should be noted that direct observation of an ordered lithium lattice complicated by the relatively small scattering section of lithium as compared with Ta and Te atoms. However, for lighter elements such as Ti and S, diffuse X-ray diffraction data has been used to confirm the electrochemical results obtained on TiS_2.[16]

The fractional compositions defining ordered intermediates in $TaTe_2$ differ notably from those found in TiS_2 ($1/9$, $1/4$, $5/7$, $4/5$, and $6/7$). For TiS_2, these values give place to definite superstructures in which the lattice energy can be derived by taking into account only nearest-neighbor interactions.[16] As all the octahedral sites located at the van der Waals interlayer space are equivalent in TiS_2 (1b sites of the $P\bar{3}m1$ space group), all nearest-neighbors are energetically equivalent. On the contrary, according to the structural data for $TaTe_2$,[1] the empty pseudooctahedral sites between corrugated $TaTe_2$ sandwiches are distributed in two sets of equivalent sites of different symmetry: 2d ($2/m$) and 4i (m) with $x \simeq 0.14$ and $z \simeq 0.49$. The most symmetrical sites fall between tantalum atoms that belong to the outer row of the upper and lower ribbons (i.e., displaced from the center of the Te_6 octahedra) while 4i sites have tantalum atoms in one of the adjacent slabs which are the central row of a ribbon (i.e., at the center of the Te_6 octahedron; see Figure 1). If preferential 2d site occupancy in then assumed, several new arrangements can be expected that also minimize nearest-neighbor interactions in each set of equivalent sites. These are half 2d ($x = 1/6$), all 2d ($x = 2/6$) and all 2d and half 4i ($x = 4/6$). The possible lithium-ordered phases are schematically depicted in Figure 4 and have a composition that fits well with the observed limits of the insertion regions in the discharge experiments.

On the other hand, the electron diffraction patterns for a sample with $Li_{0.2}TaTe_2$ composition showed the presence of extra spots around some spots of the basic hexagonal structure such, as $(020)_h/(910)_m$ (Figure 2c). These spots were poorly resolved, probably due to the low crystallinity of the lithiated product and the low scattering of lithium atoms. However, the distance between one basic spot and one neighbor extra spot may indicate a new periodicity of ca. 20 Å. In addition it can be observed that the extra spots differ by ca. 10−11° from $[100]_m$. For $Li_{0.17}TaTe_2$ having only half of the 2d sites occupied by lithium ions, a superstructure cell with a axis along the $[110]_m$ crystallographic direction, differing by 10.7° from a_m, and a dimension of $2a_h7^{1/2}$ could be deduced (see Figure 4, $x = 1/6$). The agreement between these values and the electron diffraction data may be interpreted as an indirect evidence of the description given to the electrochemical results.

The discharge data of $Na/NaClO_4(PC)/TaTe_2$ (Figure 3) cells shows the presence of two consecutive pseudoplateaus at 1.35 and 1.05 V located between in the $0.1 < x < 0.5$ and $0.7 < x < 1.0$ ranges, respectively. For low sodium contents the absence of a complex pattern as that found in lithium intercalation gives little evidence about the possible occurrence of sodium ordered phases. The two voltage pseudoplateaus are indicative of two different insertion processes, as evidenced by the corresponding incremental capacity peaks resolved in the step potential electrochemical spectra of the sodium cells (Figure 3). At each potential within these effects, a slow current relaxation was observed, as expected by sodium ion diffusion during the two different steps of the intercalation process. The composition limits for these successive electron plus ion injection processes are located at ca. $x = 0.6$ and $x = 1.0$, respectively.

As in $NaNbTe_2$ the XPD data of $NaTaTe_2$ can be described by using an undistorted hexagonal unit cell, $a_h x a_h$ which evidences the loss of the ribbon chain modulation. Similarly, the electron microscopy observation of lattice fringes in $Na_{0.6}TaTe_2$ particles (Figure 5) recorded at room temperature suggest the formation of a $a27^{1/2} \times a27^{1/2}$ cell. Thus, two sets of lattice fringes separated by ca. 6.3 Å and forming ca. 45° were found in surface regions of the particles, which cannot be explained on the basis of the monoclinic cell of $TaTe_2$. On the contrary, the observed expansion for this composition together with the unit-cell parameters of the in-plane $a27^{1/2} \times a27^{1/2}$ superlattice agree with the ⟨024⟩

(14) West, K.; Jacobsen, T.; Zachau-Christiansen, B.; Atlung, S. *Electrochim. Acta* **1983**, *28*, 97.
(15) Thompson, A. H. *Phys. Rev. Lett.* **1978**, *40*, 1511.
(16) Hibma, T. *J. Solid State Chem.* **1980**, *34*, 97.

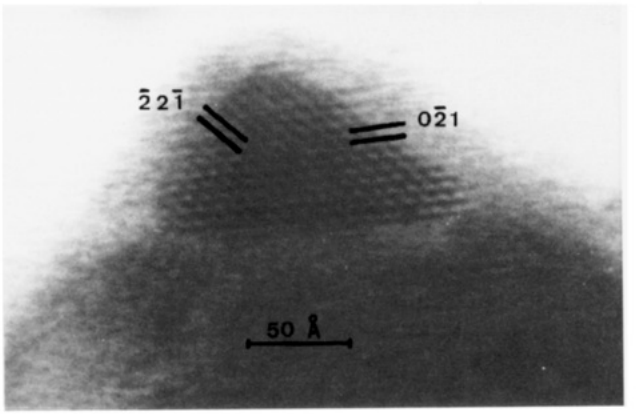

Figure 5. ⟨024⟩ zone axis bright field lattice image image of $Na_{0.6}NBTe_2$ showing 6.2 Å lattice fringes.

zone axis image suggested by the $\bar{2}2\bar{1}$ and $0\bar{2}1$ fringes in Figure 5. However, it should be noted that this structural variety does not extend throughout a given particle, probably indicating a lower stability of this modification in $TaTe_2$ as compared with $NbTe_2$.

Table 1 shows a comparison of the unit-cell parameters of group 5 ditellurides and the products of electrochemical insertion of lithium and sodium. The monoclinic structure is preserved in all cases except for sodium intercalated $NbTe_2$ and $TaTe_2$. However, it should be noted that the nature of the monoclinic distortion is reversed for $LiNbTe_2$ and $LiTaTe_2$, having $3b_m3^{1/2}$ greater than a_m, a behavior not found even by cation substitution in $TaTe_2$.[17] The fact that the ribbon chain modulation remains basically unaltered by lithium insertion in all host lattices considered here is probably a consequence of a partial covalent character of Li−Te bonding. The changes observed in a_m, b_m, and β_m may be a consequence of lattice adaptation to the changes in electron count due to partial electron donation from incoming lithium atoms. The decrease in $a_m/3{\cdot}3^{1/2}{\cdot}b_m$ for the heavy group 5 metals can be associated with a larger ionic character of the M−Te interactions which are more sharply affected by the partial electron donation from the incoming lithium atoms. On the other hand, the observed expansions in the pseudohexagonal c_h parameter normal to the layers ($c_m \sin \beta_m$) are lower for lithium intercalated products (0.35 Å ≤ Δc_h ≤ 0.59 Å). The larger values for niobium and tantalum (0.59 and 0.47 Å, respectively) are probably a consequence of the larger repulsions between lithium and transition-metal ions due to the more ionic character of these compounds. Nevertheless, these values are consistent with lithium occupancy of the distorted octahedral sites. In contrast, while the expansion found for $NaVTe_2$ (1.17 Å) is similar to that found for sodium ions in octahedral coordination (1.175 Å in $NaTiS_2$[18]), the hexagonal phases of $NaMTe_2$ (M: Nb, Ta) composition involve larger expansions (Δc_h = 1.40 and 1.24 Å, respectively) and significantly larger unit-cell volumes (Table 1). The nature of this particular distortion involves changes in the stacking of MTe_2 slabs leading to a trigonal prismatic coordination of sodium ions (Δc_h is 1.285 Å in $Na_{0.55}TiS_2$ and 1.25 Å in $Na_{0.6}TaS_2$).[18]

The standard Gibbs free energy of lithium insertion into group 5 ditellurides was evaluated as a function of composition by integration of open circuit voltage vs composition curves, according to the following expression:[8]

$$\Delta G_I^\circ = -F\int_0^x E\,dx \qquad (1)$$

which is simply Faraday's constant times the area under the voltage−composition curve from the pure chalcogenide to the intercalated compound. These results were obtained from open circuit voltage measurements, after allowing equilibrium to be reached at each composition. In addition, special care was taken to avoid the passage of significant amounts of electricity that could result in some electrical energy dissipation as Joule heat in the internal resistance of the cell during the measurements. Under these conditions, the measured voltages can be considered to be equivalent to emf values and they can be used to obtain ΔG_I°. The ΔG_I° values for lithium and sodium intercalation are plotted against x in Figure 6. The lithium intercalates have more negative standard free energies of intercalation than do the sodium-intercalated compounds, which is consistent with the general trend of the free energy of intercalation of alkali metals in transition dichalcogenides.[5−8] However, it should be noted that while lithium insertion is thermodynamically more favorable in the vanadium compound, the opposite is true for the sodium intercalates. The more negative values of ΔG_I° for Na_xNbTe_2 and Na_xTaTe_2 are consistent with the particular structural changes involved in these compositions. The results obtained for $AMTe_2$ compositions are compared with other group 5 dichalcogenides in Table 3. From these results, it is worth noting that alkali-metal insertion in the tellurides is usually less favorable than in the analogous sulfides and selenides. According to the electronic structure of the layered

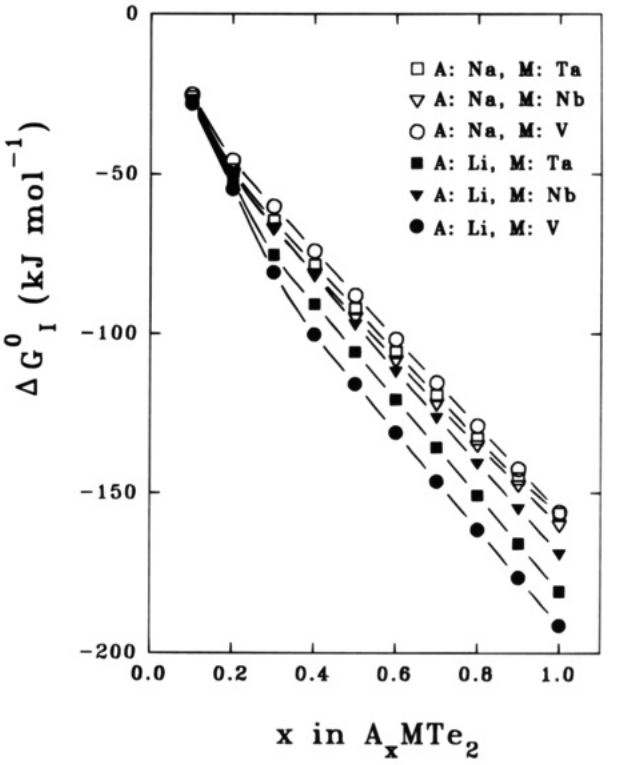

Figure 6. Plot of standard Gibbs free energy of intercalation vs composition.

(17) Lee, S.; Nagasundaram, N. *Chem. Mater.* **1989**, *1*, 597.
(18) Hibma, T. In *Intercalation Chemistry*; Whittingham, M. S., Jacobson, A. J., Eds, Academic Press: New York, 1982, p 285.

Table 3. Values of ΔG_I° at 25 °C Expressed as kJ/mol for Different Compounds of the AMX_2 (A: Li, Na; M: V, Nb, Ta; X: S, Se, Te) Series

$LiVX_2$		$LiNbX_2$		$LiTaX_2$	
$LiVS_2$	−222.2[5]			$LiTaS_2$	−211.3[6]
$LiVSe_2$	−191.2[7]	$LiNbSe_2$	−200.0[5]		
$LiVTe_2$	−191.2[a]	$LiNbTe_2$	−168.6[a]	$LiTaTe_2$	−180.5[a]
$NaVX_2$		$NaNbX_2$		$NaTaX_2$	
		$NaNbS_2$	−178.2[8]	$NaTaS_2$	−179.5[8]
$NaVTe_2$	−155.8[a]	$NaNbTe_2$	−159.9[a]	$NaTaTe_2$	−156.3[a]

[a] This work.

transition metal dichalcogenides with undistorted 1T structures, such as VS_2 and VSe_2, the t_{2g} band is expected to be one-sixth filled in group 5 compounds. For 2H-NbS_2, -$NbSe_2$, -TaS_2, and -$TaSe_2$, the trigonal prismatic coordination of transition-metal atoms split further the t_{2g} band, leaving the resulting low-lying d_{z^2} band half-filled.[18] For group 5 ditellurides, two additional effects should be taken in account. First, the Te−Te interlayer interactions rise the electron count to $d^{4/3}$,[3] thus increasing the energy of the Fermi level. Second, the splitting of the two one-third filled hidden 1-D d-block bands[4] to give metal trimerizations and the ribbon chain modulation (Figure 1) leads to filled lower energy subbands. Both effects make electron donation from the incoming alkali atoms energetically less favorable.

To obtain further evidence of the nature of the interactions between inserted ions for each studied system, the expression for the cell voltage vs x of a cell proposed by Armand[19] was applied to the data in Figure 6. For a single intercalation process, a fixed temperature and a final x value equal to unity, the equation proposed by Armand takes the form

$$E(x) = E_{1/2}^\circ - (RT/F)\ln[x/(1-x)] - (RT/F)g(x - {}^1/_2) \quad (2)$$

where $E_{1/2}^\circ$ is the emf of the cell in the standard condition $x = {}^1/_2$ and g the electrostatic repulsion factor between inserted ions. For group 5 ditellurides, the strict application of this model is limited due to the presence of consecutive ordered phases and different sites for alkali ion occupancy, in which subtle changes in electrostatic repulsion factor could be expected. Nevertheless, this equation has been successfully applied to describe the voltage vs x plots of lithium cells using TiS_2 as cathode material, irrespective of the occurrence of ordered superstructures during the intercalation process. In fact, a good linearity in the $0 < x < 1$ interval was found in a plot of $V + (RT/F)\ln[x/(1-x)]$ vs x in TiS_2 cells. The value and negative sign of the slope were used to confirm of the repulsive interactions between the incoming lithium cations and the value of interaction energy, which were in agreement with previously reported data.[20]

Moreover, an integrated form of eq 2 was used in the present study to provide an average description of the thermodynamics of the complete discharge process. In this way, the standard Gibbs free energy of alkali-metal insertion can be derived as

$$\Delta G_I^\circ = -FE_{1/2}^\circ x + RT[x\ln x + (1-x)\ln(1-x) + g(x^2 - x)/2] \quad (3)$$

Table 4. Results of the Fitting of the Integrated Form of Armand Equation to the ΔG_I° vs x Plots[a]

compound	$E_{1/2}^\circ$/V	g	compound	$E_{1/2}^\circ$/V	g
Li_xVTe_2	1.935	68.84	Na_xVTe_2	1.579	38.50
Li_xNbTe_2	1.709	46.97	Na_xNbTe_2	1.616	55.66
Li_xTaTe_2	1.824	57.26	Na_xTaTe_2	1.590	51.93

By nonlinear curve-fitting procedures to the experimental ΔG_I° data, the results showns in Table 4 were obtained. All g values were positive as expected from repulsive interactions. For lithium intercalation, the expected decrease from V to Nb as a result of the increase in c_m unit cell parameter is observed. However, the values of Na_xNbTe_2 and Na_xTaTe_2 are larger than those of Na_xVTe_2. This sequence may evidence the dramatic structural changes induced by sodium insertion in the niobium and tantalum ditelluride layers. These solids lose the modulation and thus the corrugated layers and the nonequivalent insertion sites with sodium intercalation, thus increasing repulsive interactions between sodium ions. A trigonal prismatic coordination of sodium cations is found in these compositions, which is also absent in the other intercalation compounds and may affect the interactions between ions. These effects are also responsible of the absence of a neat decrease in g from Li_xNbTe_2 to Na_xNbTe_2.

Finally, Figure 7 shows a comparison of the diffusion coefficients of lithium and sodium insertion into group 5 ditellurides. These were determined by the Honders method.[21] The method is a modified version of the galvanostatic intermittent titration technique (GITT) developed by Weppner and Huggings.[22] It allows chemical diffusion coefficients to be calculated by using transient measurements, without the need for the slope of the OCV curve. In addition, the method requires no prior knowledge of the electrode surface area, which is difficult to determine in pressed powdered samples. The Honders method has been successfully applied to the determination of the diffusion coefficient of Li^+ in various positive electrodes such as TiS_2.[20,23] The method is based on the analysis of the relaxation periods which follow a long-time galvanostatic current pulse through a Li/electrolyte intercalation electrode cell. When the following conditions are fulfilled: $\tau_{pulse} > 0.25$ and $\tau_{decay} < 0.25$ (where $\tau = \tilde{D}t/\delta^2$), and for small relaxation time values, the chemical diffusion coefficient $\tilde{D}$ can be expressed as

$$\tilde{D} = 4/\pi[\delta(d\Delta E'/dt)/(d\Delta E/\sqrt{t})]^2 \quad (4)$$

where ΔE are the changes in cell voltage during cell relaxation, $\Delta E'$ the difference between ΔE and the straight line obtained by extrapolating the linear part of the ΔE vs $\sqrt{t}$ plot, and δ the cathode thickness. For the determination of diffusion coefficients, 0.3−0.5 mm diameter cathode pellets and current pulses in the range

(19) Armand, M. B. *Materials for Advanced Batteries*; Murphy, D. W., Broadhead, J., Steele, B. C. H., Eds.; NATO Series; 1980; p 145.
(20) Julien, C. In *Microionics Solid State Integrable Batteries*; Elsevier Science Publishers: Amsterdam, 1991, p 309.
(21) Honders, A.; Der Kinderen, J. M.; Van Heeren, A. H.; Wit, J. H. W.; Broers, G. H. J. *Solid State Ionics* **1985**, *15*, 265.
(22) Weppner, W.; Huggins, R. A. *J. Electrochem. Soc.* **1977**, *124*, 1569.
(23) Pistoia, G.; di Vona, M. L.; Tagliatesta, P. *Solid State Ionics* **1987**, *24*, 103.

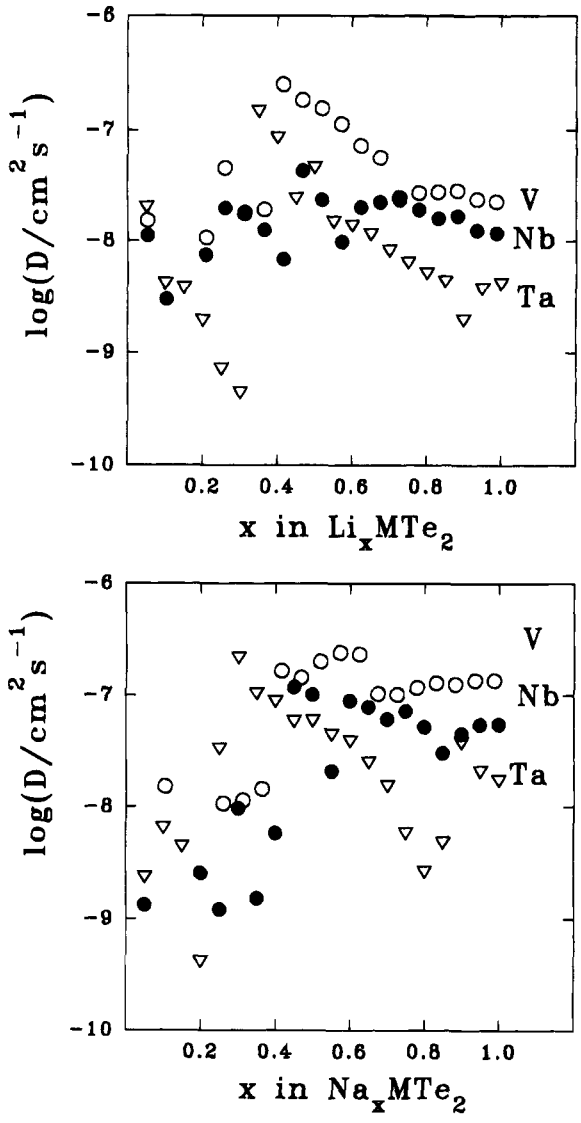

Figure 7. Plot of chemical diffusion coefficients of lithium and sodium into group 5 ditellurides.

6−15 μA/cm^2 were used, which resulted in discharges of 0.05 F. Discharge periods between 8 and 22 h were applied in order to fulfill the condition $\tau > 0.25$. Relaxation periods were interrupted when voltage changes dropped below 1 mV/h.

The results in Figure 7 show significant discontinuities in the values of the diffusion coefficients as a function of composition that may be indicative of the different sites available for intercalation. In fact, a model such as that proposed by Nagelberg[24] to explain the compositional variation of the diffusion coefficients in relatively more simple structures cannot be applied here. In that model, the diffusion of an atom involves a neighboring empty site. In the hexagonal close-packed stacking, the neighboring empty site is a tetrahedral site and is surrounded by three equivalent octahedral sites which can be occupied. Thus, the diffusion in the ideal 1T solid has only two distinct jump frequencies: one when two adjacent octahedral sites are empty, and a second smaller frequency when one adjacent site is vacant and one is filled. For the distorted 1T structure of MTe_2 the distorted octahedral sites are not energetically equivalent, and the number of distinct jump frequencies increases to five, only by taking into account the type (2d or 4i) of the adjacent octahedral vacant sites and neglecting the different tetrahedral neighboring sites. This in turn does not allow the application of a relatively simple expression of the dependence of D with x. Moreover, the irregularities found for lithium intercalation at x = 0.12, 0.3, and 0.6 may be associated with the proposed lithium-ordered phases which in turn lead to minima in the incremental capacity curve at these compositions. Thus, if a lower energy of 2d sites is assumed, fast ion diffusion is inhibited during filling of the complete set of these sites (i.e., up to $x = 0.33$), which can be considered as potential wells. Further diffusion through energetically less favorable 4i sites leads to higher D values, particularly in the $0.33 < x < 0.66$ interval, when all 2d sites are expected to be filled and 4i site occupancy is in the 0−0.5 range. Above $x = 0.66$, a significant decrease in D is expected as the probability of a vacant site decreases abruptly.

On the other hand, the fact that Na diffusion coefficients have larger values than those found for Li diffusion, particularly for large values of x, contrasts with previous studies on the alkali ion diffusion.[24] The origin of this divergence may be related with the fact that the interlayer Te−Te interactions are more affected by the intercalation of sodium ions with larger ionic radii than lithium ions. Thus, the c_h expansion decrease Te−Te contacts, thus decreasing the electron count from $d^{4/3}$ to d^1, and may inhibit ribbon chain modulation, particularly for Nb and Ta ditellurides, in which the corrugated layers transform into a nearly undistorted hexagonal structure. On the other hand, sodium intercalation induces changes in the stacking of the layers of $NbTe_2$ and $TaTe_2$, thus providing different paths for sodium ion diffusion through trigonal prismatic sites.

In conclusion, the intercalation properties of transition-metal ditellurides make possible to extend the present knowledge about intercalation materials to a particular case where the distortions resulting from metal−metal interactions condition the electrochemical insertion behavior. The results obtained so far show that the approaches previously used in models describing the behavior of more simple 1T structures are valid for the ditellurides whether the differences in crystallographic and electronic structure are taken into account.

Acknowledgment. We express our gratitude toward the CEC (Contract JOU2-CT93-0326) and CICYT (Contracts MAT94-1155-CE and MAT93-1204) for the financial support of this work and to Consejería de Educación y Ciencia de la Junta de Andalucía.

CM940497+

(24) Nagelberg, A. S. Ph.D. Thesis, University of Pennsylvania, Philadelphia, 1978; p 127.